Synthetic analysis of natural variants yields insights into the evolution and function of auxin signaling F-box proteins in *Arabidopsis thaliana*

R. Clay Wright*, Mollye L. Zahler*, Stacey R. Gerben* and Jennifer L. Nemhauser*

*Department of Biology, University of Washington, Seattle, Washington 98195-1800 USA

Running Title: Natural variation in auxin signaling F-box proteins

Keywords: synthetic biology; auxin-induced degradation; natural variation

Corresponding Author: Jennifer L. Nemhauser, HHMI Scholar, Department of Biology, University of Washington, Box 351800, Seattle, Washington 98195-1800 USA, Phone: 206.543.0753, Email: jn7@uw.edu

ABSTRACT

The evolution of complex body plans in land plants has been paralleled by gene duplication and divergence within nuclear auxin-signaling networks. A deep mechanistic understanding of auxin signaling proteins therefore may allow rational engineering of novel plant architectures. Towards that end, we analyzed natural variation in the auxin receptor F-box family of wild accessions of the reference plant *Arabidopsis thaliana* and used this information to populate a structure/function map. We used a synthetic assay to identify natural hypermorphic F-box variants, and then assayed auxin-associated phenotypes in accessions expressing these variants. To directly measure the impact of sequence variants on auxin sensitivity, we generated transgenic plants expressing the most hypermorphic natural alleles. Together, our findings link evolved sequence variation to altered molecular performance and phenotypic diversity at the organism-level. This approach demonstrates the potential for combining synthetic biology approaches with quantitative phenotypes to harness the wealth of available sequence information and guide future engineering efforts of diverse signaling pathways.

INTRODUCTION

Auxin controls many aspects of plant development and environmental adaptation. Natural and synthetic auxins have been used to control plant growth in fields, greenhouses and laboratories for nearly a century. In recent years, the gene families of biosynthetic and metabolic enzymes, transporters and perception machinery that determine the spatial, temporal and developmental specificity of auxin signals have been identified (Enders and Strader 2015). Recent work has just begun to determine

how functionally robust the auxin signaling machinery is to mutation (Yu *et al.* 2013, 2015), and to measure the propensity for mutations to produce novel plant phenotypes that result in evolutionary innovation (Delker *et al.* 2010; Rosas *et al.* 2013). As auxin effects are so wide-ranging, it is not surprising to find that significant variation exists in auxin sensitivity and auxin-induced transcription across *A. thaliana* accessions (Delker *et al.* 2010), perhaps contributing to morphological diversity. As such mapping evolutionary trajectories in auxin signaling could facilitate the engineering of numerous plant traits, such as root architecture, shoot branching or leaf venation—all traits associated with crop yield (Mathan *et al.* 2016).

Auxin is perceived by a coreceptor complex consisting of an F-box protein (TRANSPORT INHIBITOR RESPONSE1/AUXIN SIGNALING F-BOXES, TIR1/AFB; hereafter referred to as AFBs), an auxin molecule and a member of a transcriptional coreceptor/corepressor family (AUXIN/INDOLE-3-ACETIC ACID PROTEINS, Aux/IAAs) (Lavy and Estelle 2016). The F-box domain of the AFB associates with a Skp/Cullin/F-box (SCF) ubiquitin ligase complex that facilitates ubiquitination of the Aux/IAA proteins, targeting them for degradation (Lavy and Estelle 2016). In low auxin conditions, Aux/IAA proteins interact with and repress a family of transcription factors, the Auxin Response Factors (ARFs) (Guilfoyle and Hagen 2007). Auxin response genes are turned on when local auxin accumulation triggers degradation of Aux/IAAs thereby relieving the repression on ARFs.

A. thaliana has six *AFB* genes, *TIR1* and *AFB1-AFB5* (Dharmasiri *et al.* 2005a). The N-terminal F-box domain is modular and functionally conserved in TIR1 and AFB2, both of which form functional E3 ubiquitin ligase complexes with components in yeast

and animals (Nishimura *et al.* 2009; Zhang *et al.* 2015). The C-terminal domain of the AFBs is a leucine-rich repeat (LRR). LRR domains offer a highly evolvable scaffold for binding small molecules and proteins and perform diverse functions across all domains of life (Bella *et al.* 2008). The AFB LRR domain allows auxin sensing by interacting with both auxin and the Aux/IAA transcriptional repressor/co-receptor proteins (Dharmasiri *et al.* 2005a; Tan *et al.* 2007; Calderón Villalobos *et al.* 2012). The identity of the subunits and their affinity for one another governs the rate of Aux/IAA degradation which, in turn, governs transcriptional dynamics, cell fate and morphological change (Dreher *et al.* 2006; Pierre-Jerome *et al.* 2014; Guseman *et al.* 2015; Galli *et al.* 2015).

Here, we paired an examination of the natural coding sequence variation in the AFB family with quantification of functional variation. We used a synthetic auxin-induced degradation assay in yeast to assess the function of natural variants in isolation from the rest of the auxin response network. Variants with altered function were then evaluated in their native context by quantifying auxin-associated root growth inhibition in accessions containing these polymorphisms. Finally, we directly measured the contribution to auxin sensitivity of several of the alleles with greatest effect by generating transgenic plant lines expressing these variants under a constitutive promoter. Through this work, we have generated a higher resolution structure/function map of the AFB family and provided evidence that single polymorphisms within this family can modify plant architecture.

MATERIALS AND METHODS

Materials, media composition and general growth conditions

PCRs were performed with Phusion (cloning reactions; NEB, Ipswich, MA), GoTaq (diagnostics; Promega, Madison, WI) or GemTaq (genotyping; MGQuest, Lynnwood, WA) with primers from IDT (Coralville, Iowa). Media were standard formulations as described in (Pierre-Jerome *et al.* 2017). Plants were grown on 0.5x LS media (Caisson Laboratories, Smithfield, UT) containing 0.5% sucrose and 0.7% phytoagar (plantmedia, Dublin, OH). Seeds were obtained from the Arabidopsis Biological Resource Center (Columbus, OH).

Analysis of sequence variation

A reference dataset of the genome locations of the TIR1/AFB family and COI1 was assembled from the TAIR10 database on 28 July 2015. Transcript and coding sequences were identified using the ENSEMBL biomart version of TAIR10. The 1001 genomes Salk dataset (28 June 2010) was obtained from http://1001genomes.org/. Single nucleotide polymorphisms (SNPs) and one base pair deletions with a quality (PHRED) score of 25 and above (i.e. “quality_variant_filtered” files) were used for the following analysis using a custom R scripts unless otherwise specified. SNPs located in genes of interest were isolated and mapped to their respective gene structures using the VariantAnnotation package (Obenchain *et al.* 2014). Coding variants were identified and assembled for each gene and each accession. A dN/dS matrix of all-by-all pairs of accessions was calculated for each gene using the kaks function within the seqinr R-package (Charif and Lobry 2007), which implements the method of Nei and Gojobori (Nei and Gojobori 1986). Additionally, the genes were split into F-box and LRR

domains, with the F-box defined as the N-terminus of the protein to I50 of TIR1 and the corresponding residues of the other genes according to the alignment generated by Tan et al. (Tan *et al.* 2007). The N-terminal extension of AFB4 and 5 were excluded. Domain-wise dN/dS matrices were calculated as above. Incalculable and infinite values were excluded from these matrices prior to extraction of median values and outlier pairs. Annotated code and supplemental data are in S6 Appendix.

Strain construction

Plasmids were designed using j5 (Hillson *et al.* 2012) and constructed by aquarium (www.aquarium.bio). TIR1 and AFB2 were separately inserted into pGP8G (Havens *et al.* 2012) downstream of a GPD promoter and followed by 3X-FLAG-6X-HIS tandem affinity purification tag, via Golden Gate cloning (Engler *et al.* 2009). Mutations were introduced into the parent vectors via two-fragment Gibson assembly (Gibson *et al.* 2009). The coding sequence of the gene of interest was confirmed by sequencing (Genewiz, South Plainfield, NJ).

Plasmids were digested with *PmeI* before Lithium PEG (37) transformation into W303-1A ADE2+ yeast (MATa, leu2-3,112 trp1-1 can1-100 ura3-1 his3-11,15 ybp1-1). Correct integration of transformed colonies was confirmed by diagnostic PCR across the 3' boundary of homologous recombination, relative to the gene of interest. Similarly, pGP4GY-IAA1 and -IAA17 (Havens *et al.* 2012) were transformed into W814-29B yeast (MATα ade2-1 trp1-1 can1-100 ura3-1 leu2-3,112 his3-11,15). Confirmed transformants were struck to isolation on YPAD plates. *AFB* strains were individually mated with each *Aux/IAA* strain using standard methods (Pierre-Jerome *et al.* 2016).

Auxin-induced degradation assays in yeast

Assays were essentially as described in (Pierre-Jerome *et al.* 2017) using a BD special order cytometer with a 514 nm laser exciting fluorescence that is cutoff at 525 nm prior to PMT collection (Becton-Dickinson, Franklin Lakes, NJ). Events were annotated, subset to singlet yeast, and normalized to initial levels of fluorescence using the flowTime R package (http://www.github.com/wrightrc/flowTime). Full dataset is available via FlowRepository (http://tinyurl.com/j268y5e). Additional detail in S6 Appendix.

Root growth inhibition assays

After sterile seeds were stratified at 4ºC in the dark for 3 days (or 1 week for wild accessions), they were transferred to long day conditions at 20ºC for 4 days. Plants were then transferred to plates containing either DMSO carrier or 2,4-dichlorophenoxyactic acid (2,4-D) with root tips aligned to a reference mark. Plants were scanned after an additional 4 days of growth. Root growth was measured using ImageJ (Rasband 1997) and an Intuos Pro drawing pad (Wacom, Portland, Oregon). Additional detail in S6 Appendix.

Construction and analysis of transgenic plants

Genes of interest were inserted via Golden Gate cloning (Engler *et al.* 2009) into pGreenII (Hellens *et al.* 2000) with a pUBQ10 promoter and 3X-FLAG-6X-HIS tandem affinity purification tag. Plasmids were transformed into *Agrobacterium tumefactions* GV3101 with pSOUP (Hellens *et al.* 2000) via electroporation, and transformants were selected on plates with 50 µg/mL gentamycin and 25 µg/mL kanamycin. Plants were transformed by floral dip (Zhang *et al.* 2006), and transformants were selected on plates

with 30 µg/mL hygromycin at four days post germination after an initial light exposure for seven hours. Root growth inhibition phenotypes were quantified in T2 generation of three independent transformants as described above. Each plant was genotyped for the presence of the hygromycin resistance gene after the growth assay, using the forward primer (GATGTTGGCGACCTCGTATT) and the reverse primer (GTGCTTGACATTGGGGAGTT). Additional detail in the S6 Appendix.

Plasmids, strains and sequence files are available upon request or via Addgene. All code used to perform analysis and visualization is provided in S6 Appendix. All data including raw images are available upon request.

RESULTS

We identified polymorphisms across the entire AFB gene family in the 170 *A. thaliana* accessions of the SALK subset of the 1001 Genomes Project (Schmitz *et al.* 2013). We found 1,631 polymorphisms within coding regions, and, of these, 273 polymorphisms were predicted to result in amino acid substitutions (Table 1 and S1 Fig). *AFB3* had the highest level of nonsynonymous mutation relative to synonymous mutation, suggesting it may be undergoing neo-functionalization. *AFB4*, critical for response to the synthetic auxin picloram (Prigge *et al.* 2016), had the largest number of coding sequence polymorphisms (more than 15X the number found in *TIR1*) and the largest number of nonsynonymous polymorphisms (18X the number in *TIR1*) including the only two nonsense polymorphisms identified in this dataset. In contrast, *AFB1*, which is largely incapable of forming a functional SCF complex (Yu *et al.* 2015), has very similar ratio of nonsynonymous to synonymous changes as *TIR1*. Many of the

accessions contained nonsynonymous polymorphisms in multiple members of the AFB family (S2 Table). These additional mutations tended to occur more frequently in sister pairs (TIR1 and AFB1, AFB2 and AFB3, AFB4 and AFB5).

None of the identified accessions have nonsynonymous polymorphisms in both *TIR1* and *AFB2* (S2 Table). This may mean that *AFB2* and *TIR1* serve partially redundant yet distinct functions, a conclusion supported by genetic analysis (Dharmasiri *et al.* 2005a; Parry *et al.* 2009). The majority of the mutations in TIR1 and AFB2 occurred in positions of high diversity across the Col-0 AFB family, and most were located in surface residues of the LRR domain (Fig 1A). The majority of these mutations spanned the exterior helices and loops of the fourth through eighth LRRs (Fig 1C). This region was recently identified as being responsible for SCF^{TIR1} dimerization (Dezfulian *et al.* 2016) and is also proximal to the S-nitrosylation site (Terrile *et al.* 2012). A pair of mutations exists on the surface spanning the final three LRRs and the C-terminal cap (Fig 1D). This region may interact with the KR motif known to strongly affect auxin-induced degradation rates (Dreher *et al.* 2006; Moss *et al.* 2015). A final pair of mutations was found on the interior surface of the LRR domain horseshoe (Fig 1E).

Synthetic yeast assays reveal functional variation in TIR1 and AFB2

An auxin-induced degradation assay has been established in yeast using heterologous expression of either *TIR1* or *AFB2* (Havens *et al.* 2012). We used this synthetic assay to quantify the function of AFB natural variants in the absence of the potentially confounding effects of feedback from the auxin pathway itself or from modulation by other integrating pathways. Natural variants were engineered into the Col-0 reference sequence with co-occurring polymorphisms cloned individually and in

combination. Each AFB was then constitutively co-expressed in yeast with fluorescently labeled Aux/IAA targets. Auxin-induced degradation was measured for two targets, IAA1 and IAA17, as these substrates show distinct patterns of behavior when assayed with Col-0 TIR1 and AFB2. $TIR1^{Col}$ induces degradation of IAA1 and IAA17 at similar rates, while $AFB2^{Col}$ causes IAA17 to degrade much faster than what is observed for IAA1 (Havens *et al.* 2012). We focused on polymorphisms in the LRR domain that were predicted to be functionally divergent (having any pairwise d_N/d_S value greater than one), but analysis of the few additional polymorphisms is shown in Figures S4 and S5.

Some natural variants increased function compared to the Col-0 reference, while others decreased or nearly abrogated function (referred to hereafter as hypermorphs, hypomorphs and amorphs, respectively) (Fig 2). Of the *TIR1* polymorphisms, T154S was hypermorphic and E239K-S546L was strongly hypomorphic (Fig 2A). E239K alone was nearly amorphic, and adding S546L only slightly restored activity. T491R was the only clear hypermorph identified among the *AFB2* polymorphisms (Fig 2B). D176E was slightly hypermorphic, whereas A254V was a moderate hypomorph. In combination, these two mutations were largely additive, giving a response quite similar to $AFB2^{Col}$. $AFB2^{Q169L}$ was also a moderate hypomorph. Two *AFB2* alleles, R396C and R204K, were strong hypomorphs, and T179M was amorphic in our assays. Interestingly, the two most highly represented variants, $TIR1^{T154S}$ (present in 5 accessions) and $AFB2^{R204K}$ (6 accessions), show strong functional divergence from their respective wild-type proteins.

Accessions containing a hypermorphic *TIR1* allele are hypersensitive to auxin

We next assessed whether the functional variation observed in the synthetic assays was manifested in phenotypic differences in the respective accessions. To do this, we measured inhibition of primary root growth in the presence of exogenous auxin, a bioassay that has been used extensively to identify and characterize mutants in the *AFB* gene family (Gray *et al.* 1999; Dharmasiri *et al.* 2005a; b; Parry *et al.* 2009). We fit a log-logistic dose response model to the data to allow a more precise comparison. One parameter, the effective dose of auxin required to elicit fifty percent of the maximum root growth inhibition (ED50), was the most effective metric for differentiating among the genotypes we assayed. Two *tir1* mutants in the Col-0 background (a point mutation *tir1-1* and a null insertion *tir1-10*) were also included in our analysis. Both mutants had significantly higher ED50s as expected (Fig 3A and C). A loss of function *afb2* allele did not significantly affect the root growth response in our assays, although *tir1-1 afb2-3* double mutants had a much larger ED50 than the *tir1-1* single mutant.

In general, the root growth response of the accessions we analyzed was only subtly different from that of Col-0 (S6 Appendix, pg. 38-40), with one notable exception. Four out of five accessions carrying $TIR1^{T154S}$ were hypersensitive to auxin, following the pattern predicted by the hypermorphic behavior of that variant in yeast (Fig 3B and C). This led us to hypothesize that the $TIR1^{T154S}$ acts as a natural gain-of-function allele with the capacity to impact organ-level auxin responses.

A common *TIR1* allele confers auxin hypersensitivity to Col-0

We next generated transgenic Col-0 lines expressing $TIR1^{Col}$ or $TIR1^{T154S}$ under a constitutive promoter to quantify the phenotypic effect of $TIR1^{T154S}$. As was observed in yeast and in the wild accessions, $TIR1^{T154S}$ increased auxin sensitivity relative to $TIR1^{Col}$ (Fig 3D) in root inhibition bioassays (e.g., 20 nm 2,4-D, $p < 10^{-6}$, full statistical analysis shown in S6 Appendix). The trend of increased sensitivity conferred by $TIR1^{T154S}$ could be observed even in the absence of exogenous auxin, suggesting a differential response to endogenous auxin levels.

We similarly quantified the effect of $AFB2^{T491R}$, the only hypermorphic *AFB* variant we identified. These plants had somewhat shorter roots than plants expressing $AFB2^{Col}$ under low auxin and mock treatments. While $AFB2^{T491R}$ had a significant effect on root growth inhibition compared with $AFB2^{Col}$ ($p = 0.009$), the interaction between transgene and treatment was not significant. This is consistent with the finding that the hypersensitive response of $AFB2^{T491R}$ was strongest in the absence of exogenous auxin and became undetectable at high auxin levels—the opposite trend as what was observed with $TIR1^{T154S}$. One possibility is that these results reflect a degree of specialization in *TIR1* and *AFB2* responses at distinct auxin dosages. In support of that hypothesis, loss of *AFB2* function had a much weaker affect on root growth compared with loss of *TIR1*, but the combination was strongly auxin resistant (Fig 3A and C)(Dharmasiri *et al.* 2005a).

Dimerization domain variation affects dominance relations between TIR1 alleles

One of the unexpected findings in our analysis of auxin response across genotypes was a subtle but highly reproducible difference between the two induced alleles of *tir1* in the Col-0 background (Fig 3A, C). The point mutation *tir1-1* showed a consistently stronger loss of auxin sensitivity than the T-DNA insertion *tir1-10*, raising the possibility that *tir1-1* might be acting as a dominant negative or antimorph rather than as a simple loss-of function. In support of that interpretation, *tir1-1* mutants are semi-dominant (Ruegger *et al.* 1998), and the *tir1-1* allele (*G147D*) and several other mutations in nearby residues negatively affect SCF^{TIR1} dimerization and activity (Dezfulian *et al.* 2016).

We turned to the yeast synthetic system to further investigate this question. By transforming a single copy of each allele into haploid yeast strains of each mating type, we created all pairs of alleles via mating. We also created $tir1^{K159*}$ a mimic of the *tir1-10* T-DNA insertion allele. As expected, $tir1^{K159*}$ was an amorph, behaving similarly to an empty expression cassette (S5 Fig). *TIR1* dosage had little effect on auxin response in these assays, as *TIR1/tir1-10* heterozygotes responded similarly to *TIR1* homozygotes (Fig 4A). In contrast, expression of *tir1-1* completely abrogated *TIR1* activity (Fig 4B), providing strong evidence that *tir1-1* is indeed a dominant negative allele.

DISCUSSION

The analysis of intraspecific variation in auxin sensitivity presented here critically extends previous work on the evolution of this pathway by focusing on protein level

functional variation. Synthetic assays allowed for direct quantification of differences in the ability of TIR1 and AFB2 variants to facilitate ubiquitin-mediated degradation of their substrates. The creation of a structure/function map of natural variation revealed several areas of the F-box-LRR protein scaffold that can accommodate mutations, while modulating auxin sensitivity. This analysis further underscored the importance of the AFB dimerization domain (Dezfulian *et al.* 2016) to regulate SCF activity.

The *AFB* family provides a test case for genome evolution after gene duplication, as there is evidence of both significant novelty and redundancy between family members (Dharmasiri *et al.* 2005a; Walsh *et al.* 2006; Parry *et al.* 2009; Hu *et al.* 2012). Analysis of coding sequence polymorphisms in this study revealed significant differences across the gene family. These apparent differences in evolutionary trajectories raise the possibility for lineage-specific functional specialization. In support of this idea, several of the polymorphisms analyzed here were found in multiple accessions across a wide geographic area. These accessions, as well as those accessions with phenotypes not predicted by our synthetic functional analysis, should facilitate future examination of evolutionary robustness and plasticity in nuclear auxin signaling and downstream gene networks.

Functional diversification is occurring within the *Arabidopsis TIR1* lineage. Differences observed in *TIR1* variants analyzed in isolation in synthetic assays were frequently predictive of plant phenotype, pointing to a potential role for divergence in receptor function in allowing for optimization of auxin responses in new environments. The integrated biochemical and phenotypic analysis of natural variants refined the map of functionally relevant residues in TIR1 and AFB2, as well as generated hypotheses

about differential evolutionary paths for different *AFB* family members. This information, along with the general evolvability of the LRR scaffold (Bella *et al.* 2008), make the AFBs prime candidates for engineering novel traits in crops.

ACKNOWLEDGEMENTS

We thank Doug Fowler, Adam Leaché and Eric Klavins for guidance on methods, analysis and interpretation of our findings; members of the Nemhauser, Klavins and Imaizumi Labs for helpful discussions; and Brenda Martinez for technical assistance. This work was supported by the National Institute of Health (R01-GM107084), the National Science Foundation (MCB-1411949) and the Howard Hughes Medical Institute. R.C.W. received fellowship support from the National Science Foundation (DBI-1402222).

REFERENCES

Bella J., Hindle K. L., McEwan P. A., Lovell S. C., 2008 The leucine-rich repeat structure. Cell. Mol. Life Sci. 65: 2307–2333.

Calderón Villalobos L. I. A., Lee S., De Oliveira C., Ivetac A., Brandt W., *et al.*, 2012 A combinatorial TIR1/AFB-Aux/IAA co-receptor system for differential sensing of auxin. Nat Chem Biol 8: 477–85.

Charif D., Lobry J. R., 2007 SeqinR 1.0-2: a contributed package to the R project for statistical computing devoted to biological sequences retrieval and analysis. In: Bastolla U, Porto M, Roman HE, Vendruscolo M (Eds.), *Structural approaches to sequence evolution: Molecules, networks, populations*, Biological and Medical Physics, Biomedical Engineering. Springer Verlag, New York, pp. 207–232.

Delker C., Pöschl Y., Raschke A., Ullrich K., Ettingshausen S., *et al.*, 2010 Natural Variation of Transcriptional Auxin Response Networks in Arabidopsis thaliana. Plant Cell 22: 2184–2200.

Dezfulian M. H., Jalili E., Roberto D. K. A., Moss B. L., Khoo K., *et al.*, 2016 Oligomerization of SCF TIR1 Is Essential for Aux/IAA Degradation and Auxin Signaling in Arabidopsis. PLOS Genet 12: e1006301.

Dharmasiri N., Dharmasiri S., Weijers D., Lechner E., Yamada M., *et al.*, 2005a Plant Development Is Regulated by a Family of Auxin Receptor F Box Proteins. Dev. Cell 9: 109–119.

Dharmasiri N., Dharmasiri S., Estelle M., 2005b The F-box protein TIR1 is an auxin receptor. Nature 435: 441–445.

Dreher K. A., Brown J., Saw R. E., Callis J., 2006 The Arabidopsis Aux/IAA Protein Family Has Diversified in Degradation and Auxin Responsiveness. Plant Cell 18: 699–714.

Enders T. A., Strader L. C., 2015 Auxin activity: Past, present, and future. Am. J. Bot. 102: 180–196.

Engler C., Gruetzner R., Kandzia R., Marillonnet S., 2009 Golden Gate Shuffling: A One-Pot DNA Shuffling Method Based on Type IIs Restriction Enzymes. PLoS ONE 4: e5553.

Galli M., Liu Q., Moss B. L., Malcomber S., Li W., *et al.*, 2015 Auxin signaling modules regulate maize inflorescence architecture. Proc. Natl. Acad. Sci.: 201516473.

Gibson D. G., Young L., Chuang R.-Y., Venter J. C., Hutchison C. A., *et al.*, 2009 Enzymatic assembly of DNA molecules up to several hundred kilobases. Nat. Methods 6: 343–345.

Gray W. M., Pozo J. C. del, Walker L., Hobbie L., Risseeuw E., *et al.*, 1999 Identification of an SCF ubiquitin-ligase complex required for auxin response in Arabidopsis thaliana. Genes Dev 13: 1678–91.

Guilfoyle T. J., Hagen G., 2007 Auxin response factors. Curr. Opin. Plant Biol. 10: 453–460.

Guseman J. M., Hellmuth A., Lanctot A., Feldman T. P., Moss B. L., *et al.*, 2015 Auxin-induced degradation dynamics set the pace for lateral root development. Development 142: 905–909.

Havens K. A., Guseman J. M., Jang S. S., Pierre-Jerome E., Bolten N., *et al.*, 2012 A synthetic approach reveals extensive tunability of auxin signaling. Plant Physiol 160: 135–42.

Hellens R. P., Edwards E. A., Leyland N. R., Bean S., Mullineaux P. M., 2000 pGreen: a versatile and flexible binary Ti vector for Agrobacterium-mediated plant transformation. Plant Mol. Biol. 42: 819–832.

Hillson N. J., Rosengarten R. D., Keasling J. D., 2012 j5 DNA Assembly Design Automation Software. ACS Synth. Biol. 1: 14–21.

Hu Z., Keçeli M. A., Piisilä M., Li J., Survila M., *et al.*, 2012 F-box protein AFB4 plays a crucial role in plant growth, development and innate immunity. Cell Res. 22: 777–781.

Lavy M., Estelle M., 2016 Mechanisms of auxin signaling. Development 143: 3226–3229.

Mathan J., Bhattacharya J., Ranjan A., 2016 Enhancing crop yield by optimizing plant developmental features. Development 143: 3283–3294.

Moss B. L., Mao H., Guseman J. M., Hinds T. R., Hellmuth A., *et al.*, 2015 Rate Motifs Tune Auxin/Indole-3-Acetic Acid Degradation Dynamics. Plant Physiol. 169: 803–813.

Nei M., Gojobori T., 1986 Simple methods for estimating the numbers of synonymous and nonsynonymous nucleotide substitutions. Mol. Biol. Evol. 3: 418–426.

Nishimura K., Fukagawa T., Takisawa H., Kakimoto T., Kanemaki M., 2009 An auxin-based degron system for the rapid depletion of proteins in nonplant cells. Nat. Methods 6: 917–922.

Obenchain V., Lawrence M., Carey V., Gogarten S., Shannon P., *et al.*, 2014 VariantAnnotation: a Bioconductor package for exploration and annotation of genetic variants. Bioinformatics 30: 2076–2078.

Parry G., Calderon-Villalobos L. I., Prigge M., Peret B., Dharmasiri S., *et al.*, 2009 Complex regulation of the TIR1/AFB family of auxin receptors. Proc. Natl. Acad. Sci. 106: 22540–22545.

Pierre-Jerome E., Jang S. S., Havens K. A., Nemhauser J. L., Klavins E., 2014 Recapitulation of the forward nuclear auxin response pathway in yeast. Proc. Natl. Acad. Sci. 111: 9407–9412.

Pierre-Jerome E., Moss B. L., Lanctot A., Hageman A., Nemhauser J. L., 2016 Functional analysis of molecular interactions in synthetic auxin response circuits. Proc. Natl. Acad. Sci. U. S. A. 113: 11354–11359.

Pierre-Jerome E., Wright R. C., Nemhauser J., 2017 Characterizing Auxin Response Circuits in Saccharomyces cerevisiae by Flow Cytometry. In: Kleine-Vehn J, Sauer M (Eds.), *Plant Hormones*, Methods in Molecular Biology. Springer New York, pp. 271–281.

Prigge M. J., Greenham K., Zhang Y., Santner A., Castillejo C., *et al.*, 2016 The Arabidopsis Auxin Receptor F-Box Proteins AFB4 and AFB5 Are Required for Response to the Synthetic Auxin Picloram. G3 GenesGenomesGenetics 6: 1383–1390.

Rasband W., 1997 *ImageJ*. U. S. National Institutes of Health, Bethesda, Maryland, USA.

Rosas U., Cibrian-Jaramillo A., Ristova D., Banta J. A., Gifford M. L., *et al.*, 2013 Integration of responses within and across Arabidopsis natural accessions uncovers loci controlling root systems architecture. Proc. Natl. Acad. Sci. 110: 15133–15138.

Ruegger M., Dewey E., Gray W. M., Hobbie L., Turner J., *et al.*, 1998 The TIR1 protein of Arabidopsis functions in auxin response and is related to human SKP2 and yeast Grr1p. Genes Dev. 12: 198–207.

Schmitz R. J., Schultz M. D., Urich M. A., Nery J. R., Pelizzola M., *et al.*, 2013 Patterns of population epigenomic diversity. Nature 495: 193–198.

Tan X., Calderon-Villalobos L. I. A., Sharon M., Zheng C., Robinson C. V., *et al.*, 2007 Mechanism of auxin perception by the TIR1 ubiquitin ligase. Nature 446: 640–5.

Terrile M. C., París R., Calderón-Villalobos L. I. A., Iglesias M. J., Lamattina L., *et al.*, 2012 Nitric oxide influences auxin signaling through S-nitrosylation of the Arabidopsis TRANSPORT INHIBITOR RESPONSE 1 auxin receptor. Plant J. Cell Mol. Biol. 70: 492–500.

Walsh T. A., Neal R., Merlo A. O., Honma M., Hicks G. R., *et al.*, 2006 Mutations in an Auxin Receptor Homolog AFB5 and in SGT1b Confer Resistance to Synthetic Picolinate Auxins and Not to 2,4-Dichlorophenoxyacetic Acid or Indole-3-Acetic Acid in Arabidopsis. Plant Physiol. 142: 542–552.

Yu H., Moss B. L., Jang S. S., Prigge M., Klavins E., *et al.*, 2013 Mutations in the TIR1 Auxin Receptor That Increase Affinity for Auxin/Indole-3-Acetic Acid Proteins Result in Auxin Hypersensitivity. Plant Physiol. 162: 295–303.

Yu H., Zhang Y., Moss B. L., Bargmann B. O. R., Wang R., *et al.*, 2015 Untethering the TIR1 auxin receptor from the SCF complex increases its stability and inhibits auxin response. Nat. Plants 1: 14030.

Zhang X., Henriques R., Lin S., Niu Q., Chua N., 2006 Agrobacterium-mediated transformation of Arabidopsis thaliana using the floral dip method. Nat. Protoc. 1: 641–6.

Zhang L., Ward J. D., Cheng Z., Dernburg A. F., 2015 The auxin-inducible degradation (AID) system enables versatile conditional protein depletion in C. elegans. Dev. Camb. Engl.

1

2

FIGURE CAPTIONS

Fig 1. Clusters of natural variation in *TIR1* and *AFB2*. (A) Identified mutations tend to occur in residues of high diversity within the *Arabidopsis* AFB family. A top down view of the LRR domain of the TIR1 structure (PDB:2P1Q) is shown with the F-box domain in the bottom right and the LRR domain spiraling counterclockwise. The backbone of the TIR1 structure (Tan *et al.* 2007) was colored according to protein sequence diversity with conserved residues in blue and diverging residues in red. Diversity was calculated as Shannon Entropy using an alignment of the protein sequences of the *Arabidopsis* AFB family (TIR1, AFB1-5). All mutations are shown as sticks. AFB2 variants are in light blue and TIR1 variants are in purple. Previously identified TIR1 mutants are in dark blue (Ruegger *et al.* 1998; Yu *et al.* 2013). The IAA7 degron is shown as a light green ribbon with side-chains as sticks. The N-terminal residue of the IAA7 degron is in lighter green and the C-terminal residue is darker green. Circles around polymorphisms match the detailed views shown in panels C, D and E. (B) Mutations face the Cullin subunit of the predicted SCF^{TIR1} structure. ASK1 (light grey) was aligned with SKP1 from the human SKP2-SKP1-Cul1-RBX1 structure (PDB: 1LDK, shown in dark grey), docking with TIR1 (gold). Putative E2 location is labeled. (C) The dimerization domain on the N-terminal side of the LRR horseshoe contains the majority of natural variation in *TIR1* and *AFB2*. The *tir1-1* allele ($tir1^{G147D}$) is in light purple. (D) Two variants were located on the C-terminal side of the LRR close to the N-terminus of the degron. (E) Two additional variants were located inside the LRR horseshoe, near the inositol-hexakisphosphate cofactor.

Fig 2. Synthetic assays reveal significant functional variation in naturally occurring *AFB* polymorphisms. Nonsynonymous mutations in the LRR domains of *TIR1* (A) and *AFB2* (B) with dN/dS values >1 were synthesized and co-expressed in yeast with fluorescently labeled IAA1 or IAA17. Degradation was assessed using flow cytometry on cultures exposed to different concentrations of the auxin indole-3-acetic acid (IAA) for one hour. Error bars represent 95% confidence intervals around the median fluorescence calculated from three independent experiments. In many cases, intervals are small enough that they appear as a single line. The reference Col-0 variant is shown in grey.

Fig 3. Auxin sensitivity varies only subtly in wild accessions. (A) The impact of auxin on root growth (normalized to mock treated controls) was measured in 8-day-old seedlings. Each measurement is shown

as a transparent grey point. Solid lines represent fits from a log-logistic dose response model with a lighter ribbon indicating 95% confidence intervals. The Col-0 curve is reproduced in light grey in each panel to facilitate comparisons. (A) Assays on the reference accession Col-0, and mutants in the Col-0 background, are shown (B) Auxin sensitivity of accessions containing the hypermorphic *TIR1*^{T154S} allele. (C) Estimated ED50 values for selected accessions and controls. Parameters were compared to Col-0 values and Student's t-tests were used to estimate the likelihood that the ratio of parameters equals 1. P-values were corrected for multiple testing using the Benjamini-Hochberg method. (D) Some natural polymorphisms were sufficient to alter auxin sensitivity in plants. Mean root growth (large points) and 95% confidence intervals (error bars) of transgenic plants from three independent lines of Col-0 expressing either reference alleles or one of the putative hypermorphs *TIR1*^{T154S} and *AFB2*^{T491R}. All transgenes were expressed under the pUBQ10 promoter. The number of plants measured for each condition is shown above the X-axis with individual measurements indicated by small points.

Fig 4. *tir1-1 is a dominant negative allele*. Yeast expressing YFP-IAA17 and pairwise combinations of (A) *TIR1* and *tir1-10* (*tir1*^{K159*}) or (B) *TIR1* and *tir1-1* (*tir1*^{G147D}) alleles were treated with various concentrations of auxin for one hour before YFP-IAA17 fluorescence was measured by flow cytometry. Mean fluorescence +/- SE was calculated from four experiments. Some error bars are within the points.

SUPPORTING INFORMATION CAPTIONS

S1 Fig. Polymorphisms in the *AFB* genes of the 170 analyzed accessions. Using a sliding 5-codon window, synonymous (blue dotted) and nonsynonymous (red solid) polymorphisms were counted across each AFB gene for all 170 accessions. A vertical black dotted line separates the F-box and LRR domain of each gene and also identifies the target site of miR393. Nonsynonymous mutations functionally characterized in this study are indicated.

S2 Table. Accessions containing nonsynonymous variants in *TIR1* or *AFB2*.

S3 Fig. Characterization of additional *TIR1* polymorphisms. Nonsynonymous mutation in the F-box domain of *TIR1* and with dN/dS value <1 were synthesized and co-expressed in yeast with fluorescently labeled IAA1 or IAA17. Degradation was assessed using flow cytometry on cultures exposed to different

concentrations of the auxin, indole-3-acetic acid (IAA) for one hour. Error bars represent 95% confidence intervals around the median fluorescence calculated from three independent experiments. In many cases, intervals are small enough that they appear as a single line.

S4 Fig. Characterization of additional AFB2 polymorphisms. Nonsynonymous mutations in the F-box domain of AFB2 and or with dN/dS values <1 were synthesized and co-expressed in yeast with fluorescently labeled IAA1 or IAA17. Degradation was assessed using flow cytometry on cultures exposed to different concentrations of the auxin, indole-3-acetic acid (IAA) for one hour. Error bars represent 95% confidence intervals around the median fluorescence calculated from three independent experiments. In many cases, intervals are small enough that they appear as a single line.

S5 Fig. *tir1-10* is an amorph in synthetic auxin-induced degradation assays. A yeast expression cassette recapitulating the *tir1-10* allele ($TIR1^{K159*}$) was co-expressed with YFP-IAA17 as a homozygous diploid and along with full-length $TIR1^{Col}$ and an empty expression cassette (null). Each yeast strain was treated with various concentrations of auxin for one hour during log-phase growth. YFP-IAA17 fluorescence was measured by flow cytometry. Mean fluorescence +/- SE calculated from four experiments are represented by points and error bars respectively. Some error bars are within the points.

S6 Appendix. Supplemental information. Complete analytical methods, detailed protocols and additional figures for each section of the main text.

Table 1: Sequence variation in the AFB gene family.

	Pro	Splice	Intron	5' UTR	3' UTR	Coding	Nonsyn	Nonsense	Syn
TIR1	120	0	96	120	19	41	8	0	33
AFB1	40	0	23	38	123	76	12	0	64
AFB2	23	0	88	200	11	275	22	0	253
AFB3	26	0	16	123	173	122	53	0	69
AFB4	57	0	180	51	22	646	147	2	497
AFB5	15	0	107	14	412	471	31	0	440
Total	281	0	510	546	760	1631	273	2	1356

Polymorphisms with high quality support from resequenced accessions of the SALK 1001 genomes dataset were isolated and assigned to gene body locations according to TAIR10 annotations. Pro – promoter, Splice – splice site, UTR – untranslated region, Nonsyn – nonsynonymous, Syn – synonymous.

1 Figure 1

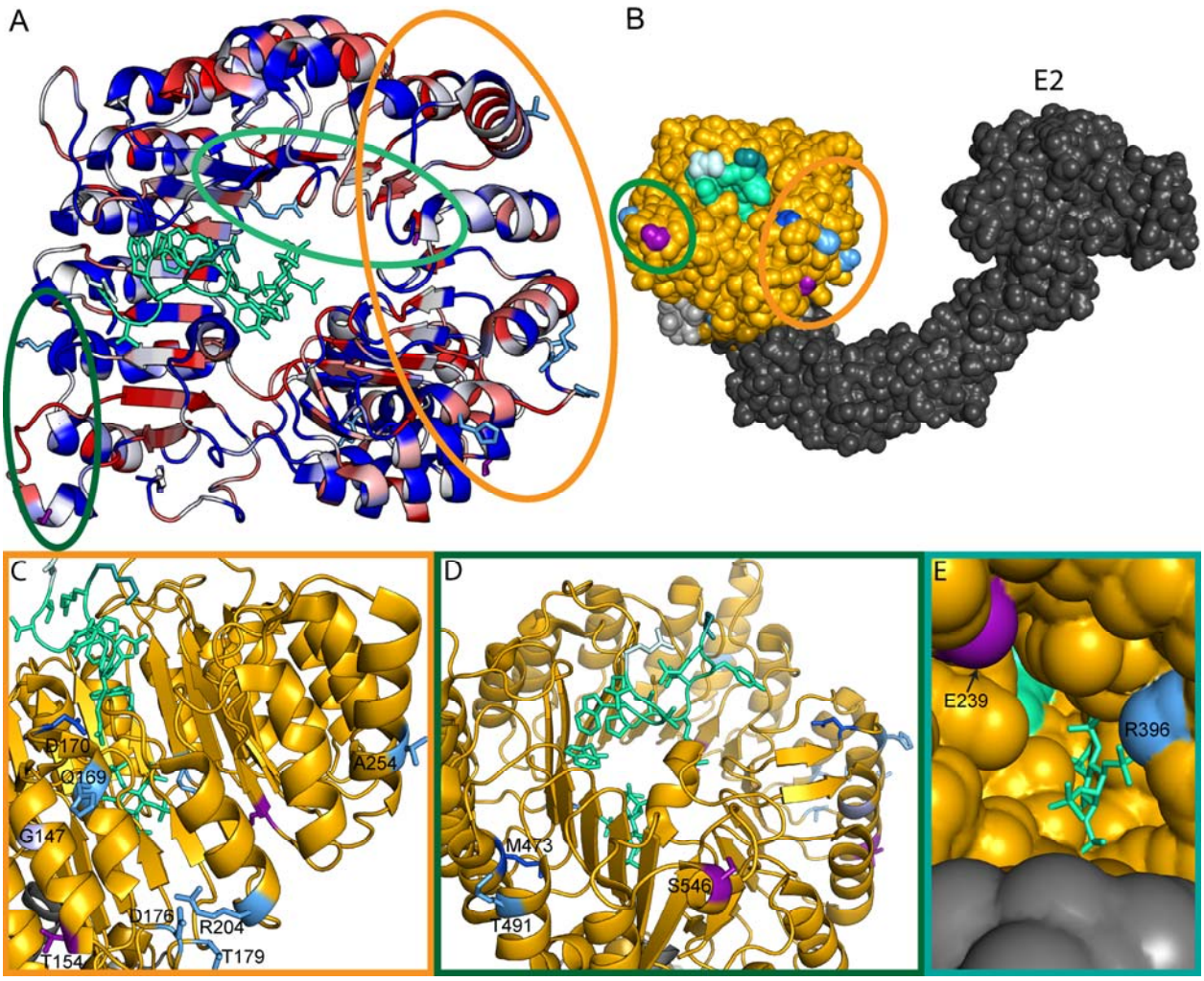

2

3

1 Figure 2

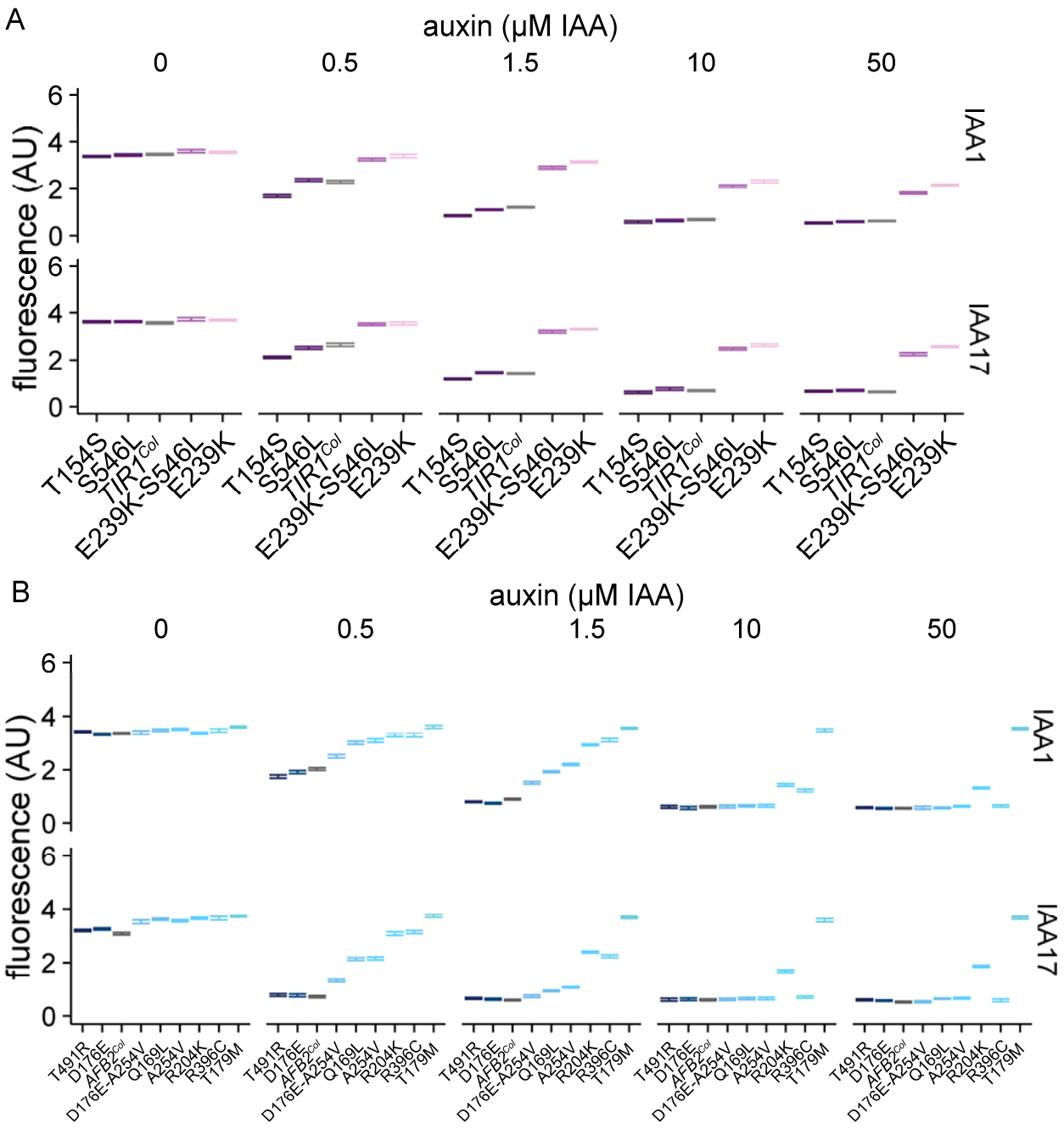

2

3

Figure 3

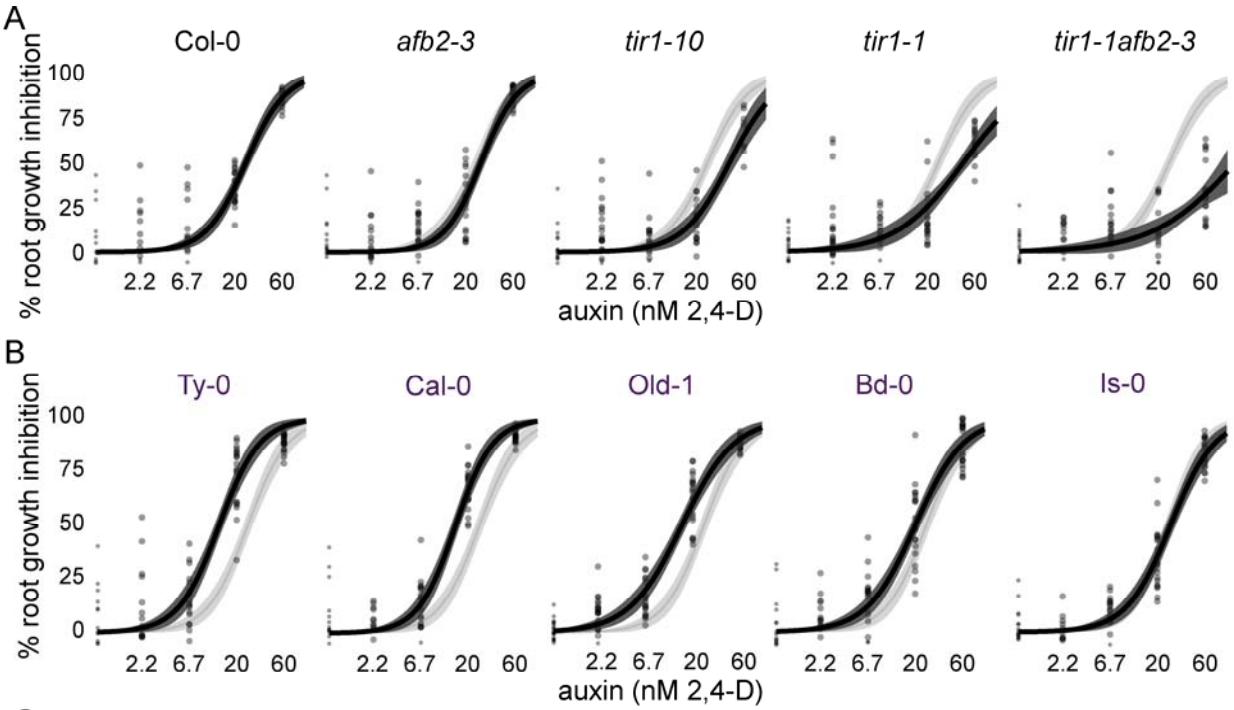

C

	gene	mutation	ED50	p-value
Ty-0	*TIR1*	T154S	13.318	<0.001
Cal-0	*TIR1*	T154S	14.872	<0.001
Old-1	*TIR1*	T154S	15.556	<0.001
Bd-0	*TIR1*	T154S	20.121	0.005
Col-0	-	-	25.922	NA
Is-0	*TIR1*	T154S	27.302	0.558
Mc-0	*TIR1*	E239K_S546L	27.910	0.538
afb2-3	*AFB2*	T-DNA	28.592	0.290
tir1-10	*TIR1*	T-DNA	43.203	<0.001
tir1-1	*TIR1*	G147D	46.238	<0.001
tir1-1afb2-3			121.753	<0.001

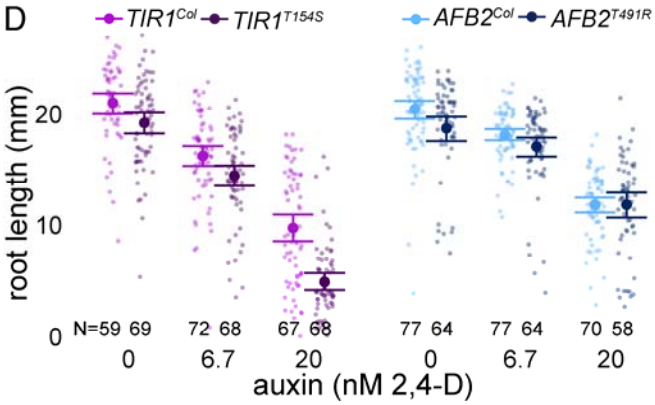

1 Figure 4

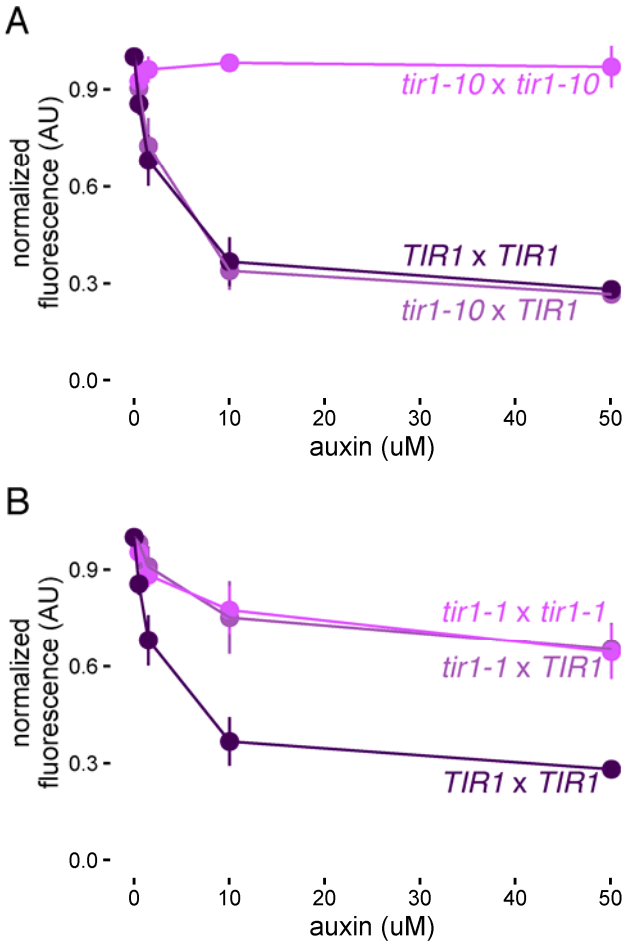

2

3

1 S1 Figure

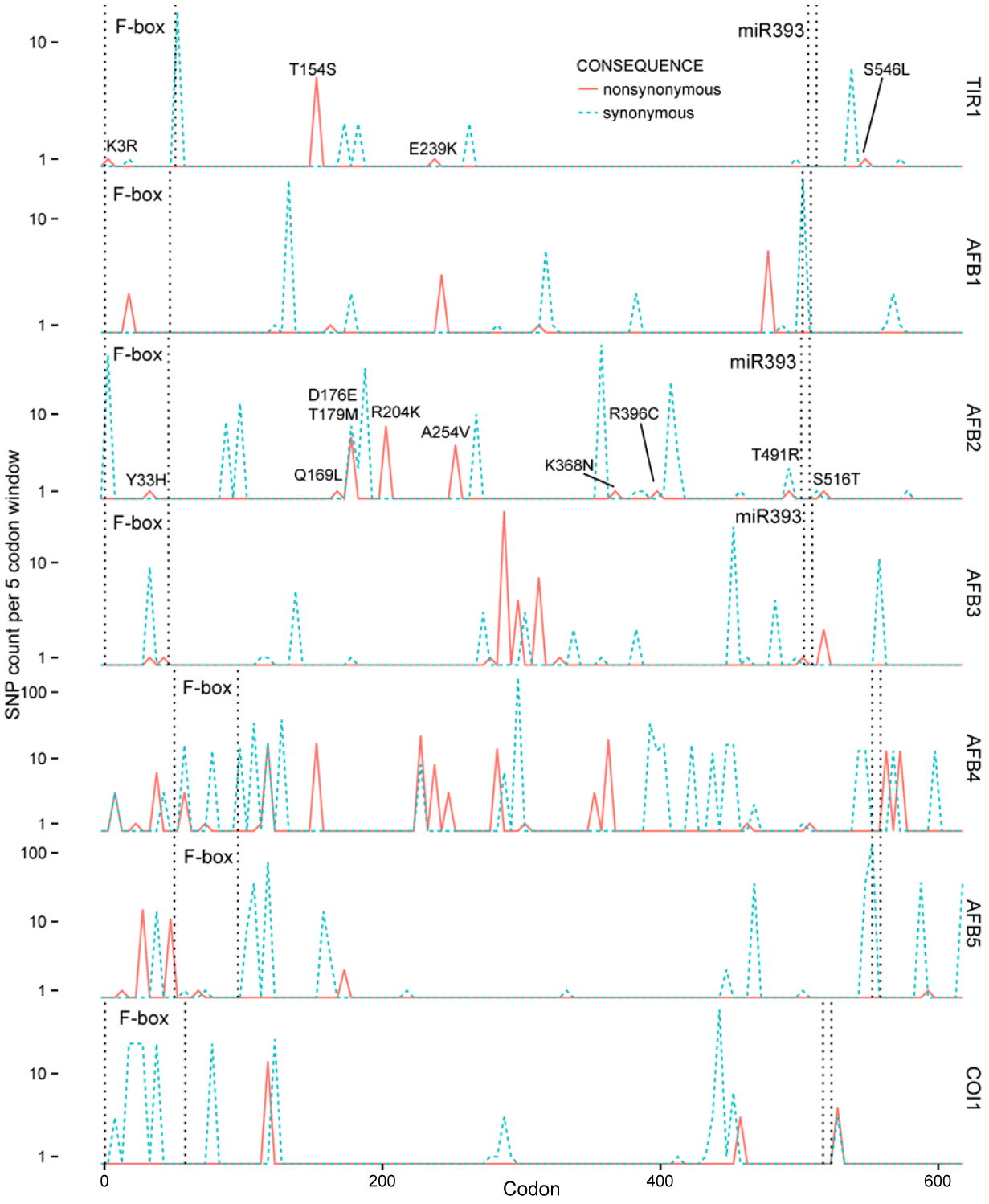

2

S2 Table: Accessions containing nonsynonymous variants in *TIR1* or *AFB2*.

accession	Germplasm	characterized mutation	*TIR1*	*AFB1*	*AFB2*	*AFB3*	*AFB4*	*AFB5*
Bd-0	CS76445	TIR1_T154S	1	0	0	1	1	0
Cal-0	CS76460	TIR1_T154S	1	1	0	1	0	0
Is-0	CS76517	TIR1_T154S	1	0	0	0	0	0
Old-1	CS76567	TIR1_T154S	1	0	0	0	0	0
Ty-0	CS76619	TIR1_T154S	1	1	0	1	2	0
Mc-0	CS76548	TIR1_E239K_S546L	2	1	0	0	2	0
Ts-1	CS76615	AFB2_Y33H_T491R	0	0	2	0	0	0
Knox-18	CS76530	AFB2_Q169L	0	0	1	1	2	1
Co-1	CS76468	AFB2_D176E_A254V	0	0	2	0	8	0
Da(1)-12	CS76470	AFB2_D176E_A254V	0	0	2	0	1	0
Dra-0	CS76476	AFB2_D176E_A254V	0	0	2	0	1	0
Bor-1	CS76453	AFB2_T179M	0	0	1	0	0	0
Gel-1	CS76492	AFB2_R204K	0	0	1	1	2	0
Gre-0	CS76497	AFB2_R204K	0	0	1	1	0	1
Pna-17	CS76575	AFB2_R204K	0	0	1	1	0	0
RRs-10	CS76592	AFB2_R204K	0	0	1	1	0	1
Tol-0	CS76614	AFB2_R204K	0	0	1	1	0	1
Tul-0	CS76618	AFB2_R204K	0	0	1	1	0	1
Br-0	CS76455	AFB2_R396C	0	1	1	2	1	0

Germplasm, variants analyzed in this study and total nonsynonymous changes for each AFB gene are indicated for each accession.

1 S3 Figure

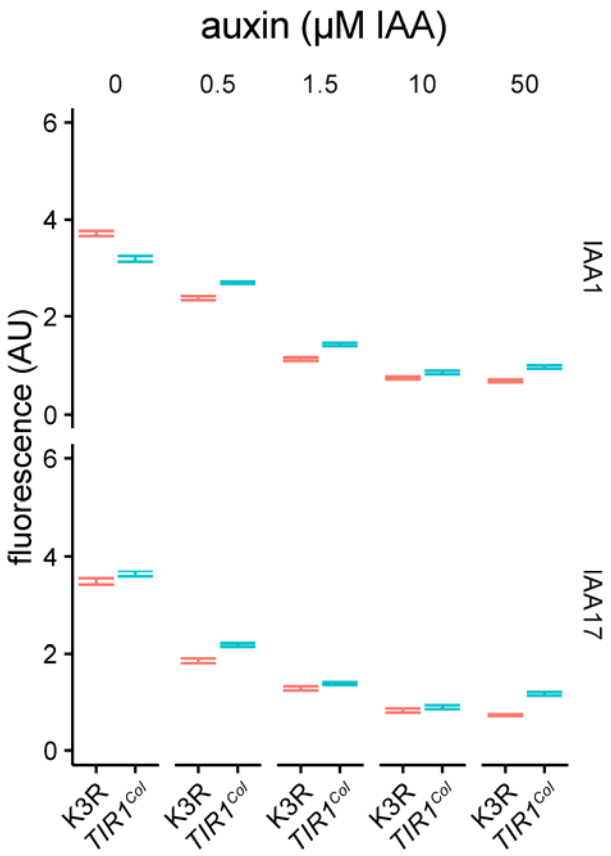

2

3

1 S4 Figure

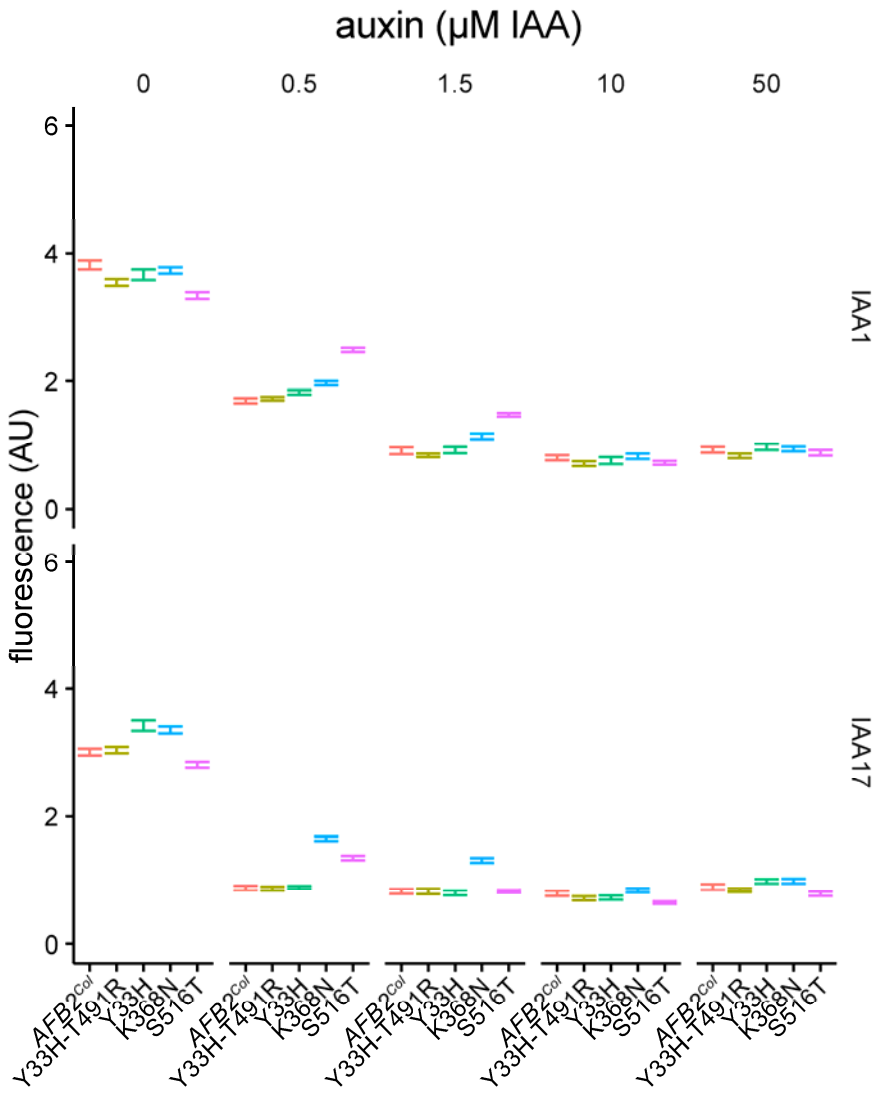

2

3

1 S5 Figure

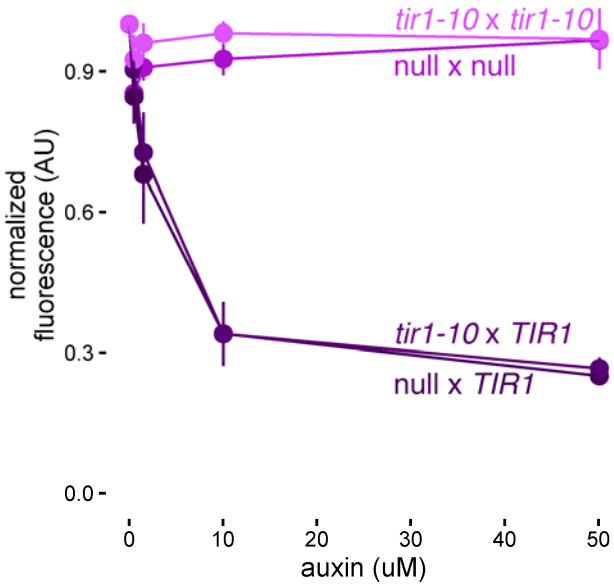

2